# Electromagnetic Scattering From a Rough Layer: Propagation-Inside-Layer Expansion Method Combined to an Updated BMIA/CAG Approach

Nicolas Déchamps and Christophe Bourlier, *Member, IEEE*

***Abstract*—An efficient method is developed to calculate the bistatic scattering coefficient (BSC) from a stack of two one-dimensional rough interfaces separating homogeneous media. The propagation-inside-layer expansion (PILE) method recently published by Déchamps *et al.* was efficient with a complexity $\mathcal{O}(N^2)$ ($N$ being the number of samples per interface). To reduce this complexity, a fast method valid for a single rough surface, the banded matrix iterative approach/canonical grid (BMIA/CAG) is combined to the PILE method. Furthermore, the calculation of the coupling interactions between both interfaces are also accelerated using a new method similar to the BMIA/CAG. The PILE method reaches then a complexity of only $\mathcal{O}(N \log N)$. A study of the convergence of the PILE is done and compared to another efficient method, the forward-backward.**

***Index Terms*—Banded matrix iterative approach (BMIA), electromagnetic scattering from rough surfaces, layered surfaces, method of moments (MoM), propagation-inside-layer expansion (PILE) method.**

## I. Introduction

THE study of electromagnetic scattering from a stack of two one-dimensional rough interfaces separating homogeneous media has a large number of applications: for example, in optics for coated surfaces, [1]–[7], in near-field microscopy [8], in remote sensing for the monitoring of oil spills [9]–[11] and in the detection of buried interfaces (e.g., in sediments) using ground-penetrating radar [12].

Both approximate and rigorous methods have been developed for 20 years to tackle this problem, but they are far less numerous than for the single-interface problem. Among the approximate methods some are based on a small perturbation method [13], on the reduced Rayleigh equations [14], both of them limited to small root-mean-square (rms) deviation of heights of the interfaces, comparatively to the wavelength. Other approximate methods are based on the geometrical optics approximation [15] and thus require quite large rms heights.

The rigorous numerical approach is more recent, due to the great number of unknowns in the double-interface configuration. Thus, only a few methods have been devoted to obtain a rigorous solution: one based on the propagation-inside-layer expansion (PILE) approach [16], one based on the extended boundary condition method (EBCM) [17], another one based on the forward-backward novel spectral acceleration (FBNSA), [18] and a last one using the steeped descent fast multipole method (SDFMM) [19]. Nevertheless, these methods have still some constraints: the method in [17] is limited to small rms heights; in the case of [19] "the depth of the underground interface should be less than one free-space wavelength to satisfy the quasiplanar structure constraint of the SDFMM." In the case of [18], the convergence domain of the method is still unclear, in particular, concerning configurations where guided waves exist. Eventually, the method in [16] is slow comparatively to the other ones (complexity of $\mathcal{O}(N^2)$ versus $\mathcal{O}(N \log N)$ and less, where $N$ is the number of samples per interface).

To overcome this limitation, we propose a fast numerical method improving PILE approach [16], which is devoted to efficiently compute the scattering from a stack of two one-dimensional (1-D) rough interfaces, and with a complexity $\mathcal{O}(N \log N)$. This method is not restricted to small rms heights nor small thicknesses $H$.

The main advantage of PILE method is that it breaks up the resolution of the linear system (obtained from the method of moments [20], [21]) into different steps; two dedicated to solve for the local interactions on the surfaces and two other ones focused on the coupling. Thus it allows the use of efficient methods valid for a single rough interface [22], [23] to calculate the local interactions. In this paper PILE is improved by adapting one fast method, the banded matrix iterative approach/canonical grid (BMIA/CAG) to both the local interactions and the coupling steps.

This paper is organized as follows: in Section II the PILE algorithm is briefly reminded. Section III focuses on the BMIA/CAG for a single interface, that is used to solve for the local interactions on each interface; the notations introduced here are helpful to clarify on the Section IV, where the coupling step of PILE is accelerated with a new method. In Section V, the convergence of the accelerated PILE method is investigated, and last, comparisons with a rigorous [18] method of the literature are presented.

## II. PILE Method

As a preliminary remark, it is worth noticing that the method developed in Section IV is efficient to speed up the calculation of the coupling between two interfaces, and therefore can be used in conjunction with other methods than PILE, as for example Jacobi methods, or conjugate gradient methods. As we

Manuscript received January 29, 2007; revised April 27, 2007.

The authors are with the Radar Team, Institut de Recherche en Electrotechnique et Electronique de Nantes Atlantique (IREENA), Polytech'Nantes, 44306 Nantes Cedex 3, France (e-mail: christophe.bourlier@univ-nantes.fr).

Digital Object Identifier 10.1109/TAP.2007.905940

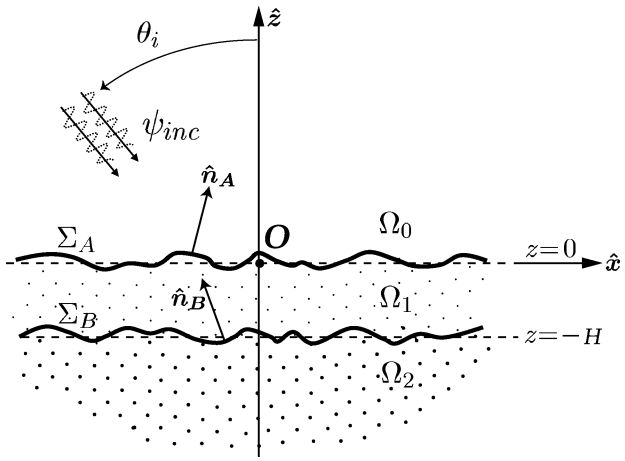


Fig. 1. Scattering from two rough interfaces $\Sigma_A$ and $\Sigma_B$ separating homogeneous media.

originally programmed this method with PILE, next we will recall the basics of PILE method.

### A. Geometry of the Problem

Let us assume that the rough layer is invariant along the $\hat{\boldsymbol{y}}$ direction and that the incident wave vector lies in the $(\hat{\boldsymbol{x}}, \hat{\boldsymbol{z}})$ plane. Consequently, the problem is two-dimensional and the layer is delimited by two one-dimensional surfaces: an upper one, $\Sigma_A$ defined by the surface equation $z = \zeta^A(x)$, and a lower one, $\Sigma_B$, defined by $\zeta^B$ (Fig. 1). $\zeta^{A,B}$ are assumed to be stochastic, stationary, Gaussian processes, satisfying $\langle \zeta^A \rangle = 0$ and $\langle \zeta^B \rangle = -H$, where $H > 0$ is the mean thickness of the layer; the surface height spectrum can be of any kind. If the surfaces are not identical, one must pay special attention to avoid any intersection between them.

The random surfaces $\Sigma_{A,B}$ can easily be generated by a spectral method, widely used in the calculation of wave scattering [21]. If $N$ represents the number of samples for each surface, the discreticized abscissa and heights of the surfaces are given by

$$x_n = -\frac{L}{2} + \left(n - \frac{1}{2}\right) \triangle x \quad \text{and} \quad \zeta^{A,B}(x_n) \quad n = 1 \ldots N \tag{1}$$

where $\triangle x = L/N$ is the sampling step and $L$ is the total length of each surface. A point of the plane $(\hat{\boldsymbol{x}}, \hat{\boldsymbol{z}})$ will be denoted by $\boldsymbol{r} = x\hat{\boldsymbol{x}} + z\hat{\boldsymbol{z}}$ and a point belonging to $\Sigma_{A,B}$ by $\boldsymbol{r_n^{A,B}} = x_n\hat{\boldsymbol{x}} + \zeta^{A,B}(x_n)\hat{\boldsymbol{z}}$. For the sake of clarity, we will let $\zeta_n^{A,B} = \zeta^{A,B}(x_n)$.

The surfaces separate three homogeneous media: the upper one, $\Omega_0$, considered as air, the intermediate one, $\Omega_1$ filling the layer, and the lower one, $\Omega_2$. $\Omega_2$ will be considered as a lossy dielectric or a perfect conductor, and we will denote the corresponding configuration, for the sake of simplicity, dielectric case or perfectly conducting case, respectively. The wave number in the medium $\Omega_j$ will be denoted $k_j$.

To avoid edge limitations, the incident field $\psi_{\text{inc}}$ is chosen as a Thorsos' tapered plane wave [24]. Since the paper is devoted to moderate incidence angles, this wave is appropriate and satisfies Maxwell's equations with good accuracy [21]. Let us denote $\theta_i$ the incident angle, defined with respect to $\hat{\boldsymbol{z}}$ in the counterclockwise direction, and $g$ the tapering parameter, which has a dimension of length and controls the spatial extent of the incident wave. Typically, $g$ is chosen to be some fraction of $L$; we used $g = L/6$ or $g = L/10$ in numerical simulations. Furthermore, we consider both TE (or $s$) and TM (or $p$) polarizations. An $e^{-i\omega t}$ time-harmonic convention is used.

### B. Propagation-Inside-Layer-Expansion (PILE) Method

This new method has been recently developed by Déchamps *et al.* in [16] and was thoroughly studied in this paper. The main equations are given.

An integral method combined to the method of moments leads to a linear system expressed as [16], [20]

$$\boldsymbol{Z}.\boldsymbol{X} = \boldsymbol{s} \tag{2}$$

where $\boldsymbol{Z}$ is the impedance matrix. The unknown vector $\boldsymbol{X}$ is equal to

$$\boldsymbol{X} = \begin{bmatrix} \boldsymbol{X}_A \\ \boldsymbol{X}_B \end{bmatrix} \tag{3}$$

with $\boldsymbol{X}_A$ and $\boldsymbol{X}_B$ containing the unknown fields $\psi_{A,B}$ and their normal derivatives $\partial\psi_{A,B}/\partial n_{A,B}$ on the upper and lower surfaces, respectively. For example

$$\boldsymbol{X}_A^t = \left[\psi_A\left(\boldsymbol{r_1^A}\right) \ldots \psi_A\left(\boldsymbol{r_N^A}\right) \; \frac{\partial\psi_A\left(\boldsymbol{r_1^A}\right)}{\partial n_A} \ldots \frac{\partial\psi_A\left(\boldsymbol{r_N^A}\right)}{\partial n_A}\right] \tag{4}$$

where $\cdot^t$ denotes the transpose operator. $\boldsymbol{X}_B$ has a similar arrangement of terms. The source term $\boldsymbol{s}$ contains information about the incident field

$$\boldsymbol{s} = \begin{bmatrix} \boldsymbol{s}_A \\ \boldsymbol{s}_B \end{bmatrix} = \begin{bmatrix} \boldsymbol{s}_A \\ \boldsymbol{0} \end{bmatrix} \tag{5}$$

with

$$\boldsymbol{s}_A^t = \left[\psi_{\text{inc}}\left(\boldsymbol{r_1^A}\right) \ldots \psi_{\text{inc}}\left(\boldsymbol{r_N^A}\right) \; 0 \ldots 0\right]. \tag{6}$$

and $\boldsymbol{s}_B = \boldsymbol{0}$, because the incident field only illuminates the upper surface.

To solve efficiently the linear system, we take advantage of the block partitioning of the impedance matrix $\boldsymbol{Z}$ which has the form [16]

$$\boldsymbol{Z} = \begin{bmatrix} \boldsymbol{Z}^A & \boldsymbol{C}^{B\to A} \\ \boldsymbol{C}^{A\to B} & \boldsymbol{Z}^B \end{bmatrix} \tag{7}$$

$\boldsymbol{Z}^A$ exactly corresponds to the impedance matrix of a single-interface problem, where the surface considered is the upper one, $\Sigma_A$. Likewise, $\boldsymbol{Z}^B$ is the impedance matrix of the single lower

TABLE I
EXAMPLES OF METHODS THAT CAN BE USED TO SPEED UP THE OPERATION $(\boldsymbol{Z})^{-1} \cdot \boldsymbol{v}$. COMPLEXITY WITH $\boldsymbol{Z}$ OF DIMENSION $N \times N$

| Method | *Complexity* |
|---|---|
| LU inversion | $\mathcal{O}(N^3)$ |
| FB | $\mathcal{O}(N^2)$ |
| One Level FMM | $\mathcal{O}(N^{3/2})$ |
| Multilevel FMM | $\mathcal{O}(N \log N)$ |
| BMIA/CAG | $\mathcal{O}(N \log N)$ |
| SDFMM | $\mathcal{O}(N)$ |
| FBNSA | $\mathcal{O}(N)$ |

surface, $\Sigma_B$. Matrices $\boldsymbol{C}^{B\to A}$ and $\boldsymbol{C}^{A\to B}$ can be seen as coupling matrices between the two interfaces $\Sigma_A$ and $\Sigma_B$. The complete expression of these matrices can be found in Appendix I.

As we usually compute the scattering field in the upper medium, only the upper scattered field $\boldsymbol{X}_A$ is needed. It is approximated by [16]

$$\boldsymbol{X}_A^{(P_{\text{pile}})} = \left[\sum_{p=0}^{P_{\text{pile}}} \boldsymbol{M}_c^p\right] \cdot (\boldsymbol{Z}^A)^{-1} \cdot \boldsymbol{s}_A = \sum_{p=0}^{P} \boldsymbol{Y}_A^{(p)} \tag{8}$$

in which

$$\begin{aligned} \boldsymbol{Y}_A^{(0)} &= (\boldsymbol{Z}^A)^{-1} \cdot \boldsymbol{s}_A \text{ for } p = 0 \\ \boldsymbol{Y}_A^{(p)} &= \boldsymbol{M}_c \cdot \boldsymbol{Y}_A^{(p-1)} \text{ for } p > 0 \end{aligned} \tag{9}$$

and $\boldsymbol{M_c}$ is the characteristic matrix of the layer defined as

$$\boldsymbol{M}_c = (\boldsymbol{Z}^A)^{-1} \cdot \boldsymbol{C}^{B\to A} \cdot (\boldsymbol{Z}^B)^{-1} \cdot \boldsymbol{C}^{A\to B}. \tag{10}$$

We define the norm $||\boldsymbol{M}_c||$ of a complex matrix by its spectral radius, i.e., the modulus of its eingenvalue which has the highest modulus. Expansion (8) is accurate if $||\boldsymbol{M}_c||$ is inferior to 1. The physical interpretation of $\boldsymbol{M}_c$ is shown in Fig. 2 of [16].

The advantage of the PILE method, [cf. (8)], is that the most complex operations, which are $(\boldsymbol{Z}^A)^{-1} \cdot \boldsymbol{u}$ and $(\boldsymbol{Z}^B)^{-1} \cdot \boldsymbol{u}$ (where $\boldsymbol{u}$ is a vector), only concerns the local interactions on each surface, respectively, upper and lower, and can be calculated by fast numerical methods that already exist for a single rough surface, like for instance the banded matrix iterative approach/canonical grid (BMIA/CAG) [27]–[31], the fast multipole method (FMM) [32], the method of multiple interactions (MOMI) [33], [34] or the forward-backward/NSA method (FBNSA) [35]–[38]. Let us recall that the advantage of all the above methods is that $(\boldsymbol{Z})^{-1}$ is never explicitly calculated.

## III. REMINDER OF THE BMIA/CAG FOR A SINGLE INTERFACE

Hence, applying one of the fast methods quoted before can speed up the calculations $(\boldsymbol{Z}^A)^{-1} \cdot \boldsymbol{u}$ and $(\boldsymbol{Z}^B)^{-1} \cdot \boldsymbol{u}$ and can reduce the complexity of both steps to less than $\mathcal{O}(N^2)$. Table I summarizes the complexity of each available method.

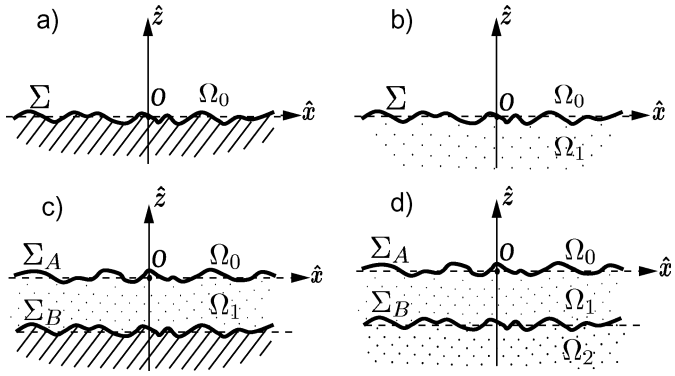


Fig. 2. Illustration of the different notations used in the paper: (a) perfectly-conducting (PC) single interface, (b) dielectric single interface, (c) PC layer, (d) dielectric layer.

The BMIA/CAG will be used in this paper because of its (relative) simplicity of programmation and its low complexity of computation. It is based on the fact that performing $\boldsymbol{Z}^{-1} \cdot \boldsymbol{u}$ is equivalent to solve $\boldsymbol{Z} \cdot \boldsymbol{v} = \boldsymbol{u}$ for $\boldsymbol{v}$; this latter problem can be solved iteratively by using a conjugate gradient scheme as BICGStab. At each iteration, it is necessary to compute $\boldsymbol{Z} \cdot \boldsymbol{v}$ where $\boldsymbol{v}$ is an updated of $\boldsymbol{Z}^{-1} \cdot \boldsymbol{u}$.

The BMIA/CAG method is employed at this step to speed up the product $\boldsymbol{Z} \cdot \boldsymbol{v}$. It was originally developed for a single perfectly conducting interface (PC), in both TE and TM polarizations [27], [28]. A quick reminder of the method will be given hereafter for these configurations. The formulas presented here are, to our knowledge, the more compact and exhaustive ones devoted to the BMIA/CAG method, and thus will be useful to anyone aiming to compute this method in an elegant manner.

Furthermore, the notations introduced here will be useful to deduce the BMIA/CAG formulas for the dielectric single-interface case and most of all, to develop the formulas for the coupling step. Fig. 2 gathers all the configurations studied. The BMIA/CAG method for the dielectric single-interface case (b) can be derived from the PC single-interface case (a), because of the particular structure of the impedance matrix for the dielectric case. In the same way, the BMIA/CAG for the coupling step (c) and (d) can be derived from case (a).

### A. TE Single-Interface Perfectly Conducting Case

Let us consider two points $(\boldsymbol{r_m}, \boldsymbol{r_n})$ belonging to the same surface $\Sigma$ and let us denote $x_d = x_m - x_n$ and $z_d = \zeta_m - \zeta_n$. $\boldsymbol{r_m}$ is the observation point, fixed, and $\boldsymbol{r_n}$ the source point, that moves on the surface. The impedance matrix $\boldsymbol{Z}$ in this configuration has the same expression as $\boldsymbol{B}^{A,B}$ in Appendix 1. We consider $x_{d0}$ the horizontal distance separating the weak interactions from the strong. $x_{d0}$ is chosen such that $x_{d0} \gg \max_{n,m=1\ldots N} |\zeta_m - \zeta_n|$; let $R_d$ be the integer part $\lfloor \cdot \rfloor$ of $x_{d0}/\Delta x$. Usually, we take $x_{d0} = 10\sigma_h$ where $\sigma_h$ is the rms height of the surface. Then, we can split up $\boldsymbol{Z}$ into

$$\boldsymbol{Z} = \boldsymbol{Z}^{(s)} + \boldsymbol{Z}^{(w)} \tag{11}$$

where $\boldsymbol{Z}^{(s)}$ is a band matrix of half-bandwidth $R_d$ representing the strong interactions, and $\boldsymbol{Z}^{(w)}$ a matrix denoting the weak interactions defined by

$$Z_{mn}^{(w)} = \begin{cases} 0 & |m-n| < R_d \\ \Delta x\, g(\boldsymbol{r_m}, \boldsymbol{r_n}) & |m-n| \geq R_d \end{cases} \tag{12}$$

where $g$ is the 2-D Green function in free space. By definition of $x_{d0}$, $x_{d0} \gg z_d$, thus the elements of $Z^{(w)}$ can be expanded as series [21], [28]

$$g(\boldsymbol{r_m}, \boldsymbol{r_n}) = \frac{i}{4} H_0^{(1)}\left(k\sqrt{x_d^2 + z_d^2}\right) \approx \sum_{p=0}^{P} a_p\left(|x_d|\right) z_d^{2p} \tag{13}$$

with

$$a_p\left(|x_d|\right) = \frac{i}{4} \frac{H_p^{(1)}\left(k|x_d|\right)}{p!} \left(\frac{-k}{2|x_d|}\right)^p. \tag{14}$$

$k$ denotes the waver number of the upper medium (the lower medium being PC) and $H_p^{(1)}$ stands for the Hankel function of the first kind of order $p$. The coefficients $a_p(|x_d|)$ can be expressed with the Hankel functions $H_0^{(1)}$ and $H_1^{(1)}$ through the relation $H_{p+1}^{(1)}(z) = (2p/z)H_p^{(1)}(z) - H_{p-1}^{(1)}(z)$ [39].

Equation (13) can be re-expressed taking into account that $z_d^{2p} = (\zeta_m - \zeta_n)^{2p} = \sum_{q=0}^{2p} C_{2p}^q \zeta_m^{2p-q}(-\zeta_n)^q$ with the binomial coefficients $C_{2p}^q = \binom{2p}{q} = (2p)!/q!(2p-q)!$.

Accordingly, the $m$-th element of the column vector $\boldsymbol{Z}^{(\boldsymbol{w})} \cdot \boldsymbol{v}$ is

$$\begin{aligned} \left(\boldsymbol{Z}^{(\boldsymbol{w})} \cdot \boldsymbol{v}\right)_m &= \sum_{\substack{0 \leq n \leq N \\ |m-n| \geq R_d}} \Delta x g(\boldsymbol{r_m}, \boldsymbol{r_n}) v_n \\ &= \underbrace{\sum_{p=0}^{P} \sum_{q=0}^{2p} \underbrace{C_{2p}^q \zeta_m^{2p-q}}_{\boldsymbol{T}_{p,q}^{(\mathrm{post})}} \sum_{\substack{0 \leq n \leq N \\ |m-n| \geq R_d}} \underbrace{\Delta x a_p\left(|x_d|\right)}_{\boldsymbol{Z}_p^{(d)}} \underbrace{(-\zeta_n)^q}_{\boldsymbol{T}_q^{(\mathrm{pre})}} v_n}_{\boldsymbol{Z}_p^{(w)}}. \end{aligned} \tag{15}$$

From this expression it is relevant to express the impedance matrix of the weak interactions by

$$\boldsymbol{Z}^{(w)} = \sum_{p=0}^{P} \boldsymbol{Z}_p^{(w)} = \sum_{p=0}^{P} \sum_{q=0}^{2p} \boldsymbol{T}_{p,q}^{(\mathrm{post})} \boldsymbol{Z}_p^{(d)} \boldsymbol{T}_q^{(\mathrm{pre})} \tag{16}$$

where $\boldsymbol{T}_q^{(\mathrm{pre})}$ and where $\boldsymbol{T}_{p,q}^{(\mathrm{post})}$ are diagonal matrices of pre- and post-multiplication, respectively, and $\boldsymbol{Z}_p^{(d)}$ is a Toeplitz matrix. These notations will be consistent throughout the paper. The elements are given by

$$\begin{aligned} \left(\boldsymbol{T}_q^{(\mathrm{pre})}\right)_{nn} &= (-\zeta_n)^q \\ \left(\boldsymbol{T}_{p,q}^{(\mathrm{post})}\right)_{mm} &= C_{2p}^q \zeta_m^{2p-q} \\ \left(\boldsymbol{Z}_p^{(d)}\right)_{mn} &= \begin{cases} \Delta x a_p\left(|x_m - x_n|\right) & \text{if } |m-n| \geq R_d \\ 0 & \text{if } |m-n| < R_d \end{cases}. \end{aligned} \tag{17}$$

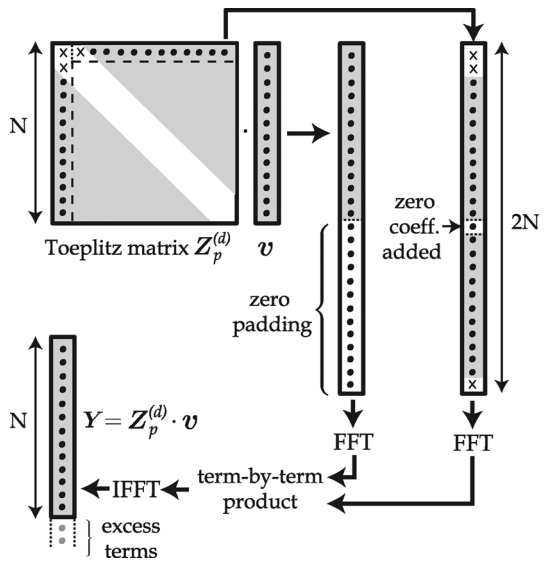


Fig. 3. Scheme of the FFT acceleration of the product $\boldsymbol{Z_p^{(d)}} \cdot \boldsymbol{v}$ when $\boldsymbol{Z_p^{(d)}}$ is a Toeplitz matrix and $\boldsymbol{v}$ a vector.

The product $\boldsymbol{Z} \cdot \boldsymbol{v}$ is then performed in two steps: first, $\boldsymbol{Z^{(s)}} \cdot \boldsymbol{v}$ is calculated without any approximation on the elements of $\boldsymbol{Z^{(s)}}$ and second, $\boldsymbol{Z^{(w)}} \cdot \boldsymbol{v}$ is calculated from (16) and (17).

Actually, the BMIA/CAG efficiency is based on the fact that $\boldsymbol{Z}_p^{(d)}$ is a *Toeplitz* matrix; all its elements $\left(\boldsymbol{Z}_p^{(d)}\right)_{mn}$ are only dependent of $|x_m - x_n| = \Delta x|m-n|$. Thus, the product $\boldsymbol{Z}_p^{(d)} \cdot \boldsymbol{v}$ can be interpreted as a convolution, and consequently, it can be accelerated by FFT (Fig. 3) [21], [28], [40]. This reduces its complexity from $\mathcal{O}(N^2)$ to $\mathcal{O}(N \log N)$.

To sum up, the product $\boldsymbol{Z^{(w)}} \cdot \boldsymbol{v}$ is a sum of different products $\boldsymbol{Z}_p^{(w)} \cdot \boldsymbol{v}$ that are performed in

$$\begin{cases} \boldsymbol{v}_1 = \boldsymbol{T}_q^{(\mathrm{pre})} \boldsymbol{v} : N \text{ operations} \\ \boldsymbol{v}_2 = \boldsymbol{Z}_p^{(d)} \boldsymbol{v}_1 : N \log N \text{ operations} \\ \boldsymbol{v}_3 = \boldsymbol{T}_{p,q}^{(\mathrm{post})} \boldsymbol{v}_2 : N \text{ operations}. \end{cases}$$

Usually, $R_d \ll N$ so the product $\boldsymbol{Z^{(s)}} \cdot \boldsymbol{v}$ of order $\mathcal{O}(R_d N)$ is less time consuming than the one involving $\boldsymbol{Z^{(w)}}$; furthermore, $P \ll N$ and accordingly, the complexity of the BMIA/CAG is $\mathcal{O}(N \log N)$.

### *B. TM Single-Interface Perfectly Conducting Case*

The impedance matrix $\boldsymbol{Z}$ in this case has a similar expression than $\boldsymbol{A}^{A,B}$ in Appendix 1. The corresponding series similar to (13) is for the TM case, for $x \geq x_{d0}$

$$\begin{aligned} -\frac{\partial g(\boldsymbol{r_m}, \boldsymbol{r_n})}{\partial n} &= -\frac{ik}{4} \frac{H_0^{(1)}\left(k\sqrt{x_d^2 + z_d^2}\right)}{\sqrt{x_d^2 + z_d^2}} \alpha_{n,m} \\ &= \sum_{p=0}^{P} \underbrace{-\frac{ik}{4} \frac{H_{p+1}^{(1)}\left(k|x_d|\right)}{p!|x_d|} \left(\frac{-k}{2|x_d|}\right)^p}_{a_p(|x_d|)} \\ &\quad \times z_d^{2p} \alpha_{n,m} \end{aligned} \tag{18}$$

where

$$\alpha_{n,m} = \zeta'_n(x_n - x_m) - (\zeta_n - \zeta_m). \tag{19}$$

The expression equivalent to (16) is more complex in the TM case because $\alpha_{n,m}$ is not symmetric with respect to $n$ and $m$

$$\boldsymbol{Z}^{(w)} = \sum_{p=0}^{P}\sum_{q=0}^{2p}\Big[\boldsymbol{T}_{p,q}^{(\mathrm{post1})}\boldsymbol{Z}_p^{(d)}\boldsymbol{T}_{p,q}^{(\mathrm{pre1})} + \boldsymbol{T}_{p,q}^{(\mathrm{post2})}\boldsymbol{Z}_p^{(d)}\boldsymbol{T}_{p,q}^{(\mathrm{pre2})} + \boldsymbol{T}_{p,q}^{(\mathrm{post3})}\boldsymbol{Z}_p^{(d)}\boldsymbol{T}_{p,q}^{(\mathrm{pre3})}\Big] \tag{20}$$

where $(\boldsymbol{T}_{p,q}^{(\mathrm{prei})})_{i=1,2,3}$ and $(\boldsymbol{T}_{p,q}^{(\mathrm{posti})})_{i=1,2,3}$ are diagonal matrices and $\boldsymbol{Z}_p^{(d)}$ is a full matrix. The elements are given by

$$\begin{aligned}
\left(\boldsymbol{T}_q^{(\mathrm{pre1})}\right)_{nn} &= (-\zeta_n)^q\,(\zeta'_n x_n - \zeta_n)\\
\left(\boldsymbol{T}_q^{(\mathrm{pre2})}\right)_{nn} &= (-\zeta_n)^q\zeta'_n\\
\left(\boldsymbol{T}_q^{(\mathrm{pre3})}\right)_{nn} &= (-\zeta_n)^q\\
\left(\boldsymbol{T}_{p,q}^{(\mathrm{post1})}\right)_{mm} &= C_{2p}^q\zeta_m^{2p-q}\\
\left(\boldsymbol{T}_{p,q}^{(\mathrm{post2})}\right)_{mm} &= -C_{2p}^q\zeta_m^{2p-q}x_m\\
\left(\boldsymbol{T}_{p,q}^{(\mathrm{post3})}\right)_{mm} &= C_{2p}^q\zeta_m^{2p-q}\zeta_m\\
\left(\boldsymbol{Z}_p^{(d)}\right)_{mn} &= \begin{cases}\Delta x a_p\left(|x_m - x_n|\right) & \text{if } |m-n| \geq R_d\\ 0 & \text{if } |m-n| < R_d\end{cases}
\end{aligned} \tag{21}$$

where $a_p$ is given by (18). As $\boldsymbol{Z}_p^{(d)}$ is a Toeplitz matrix, the complexity of the BMIA/CAG (TM and TE cases) is $\mathcal{O}(N\log N)$, although some more calculations are required for the TE case.

### C. Local Interactions in PILE Method for the Dielectric Case

The BMIA/CAG is applied in the steps $\left(\boldsymbol{Z}^A\right)^{-1}\cdot\boldsymbol{v}$ and $\left(\boldsymbol{Z}^B\right)^{-1}\cdot\boldsymbol{v}$ of the PILE method in the following way: for example, with the notation $\boldsymbol{v}^t = [\boldsymbol{v}_A^t\ \boldsymbol{v}_B^t]$

$$\boldsymbol{Z}^A\cdot\boldsymbol{v} = \begin{bmatrix}\boldsymbol{A}^{\boldsymbol{A}} & \boldsymbol{B}^{\boldsymbol{A}}\\ \boldsymbol{C}^{\boldsymbol{A}} & \boldsymbol{D}^{\boldsymbol{A}}\end{bmatrix}\begin{bmatrix}\boldsymbol{v}_A\\ \boldsymbol{v}_B\end{bmatrix} = \begin{bmatrix}\boldsymbol{A}^{\boldsymbol{A}}\cdot\boldsymbol{v}_A + \boldsymbol{B}^{\boldsymbol{A}}\cdot\boldsymbol{v}_B\\ \boldsymbol{C}^{\boldsymbol{A}}\cdot\boldsymbol{v}_A + \boldsymbol{D}^{\boldsymbol{A}}\cdot\boldsymbol{v}_B\end{bmatrix}. \tag{22}$$

$\boldsymbol{A}^{\boldsymbol{A}}\cdot\boldsymbol{v}_A$ and $\boldsymbol{C}^{\boldsymbol{A}}\cdot\boldsymbol{v}_A$ are accelerated using the BMIA/CAG for the single-interface TM PC case (Section III-B), and $\boldsymbol{B}^{\boldsymbol{A}}\cdot\boldsymbol{v}_B$ and $\boldsymbol{D}^{\boldsymbol{A}}\cdot\boldsymbol{v}_B$ are accelerated using the BMIA/CAG for the single-interface TE PC case (Section III-A). Care must be taken of the diagonal coefficients of $\boldsymbol{C}^{\boldsymbol{A}}$ which differ from those of $\boldsymbol{A}^{\boldsymbol{A}}$, and the factor $\rho_{01}$ in front of $\boldsymbol{D}^{\boldsymbol{A}}$ which depends on the polarization.

The validity domain of the BMIA/CAG is quite large: any kind of permittivity is allowed but for large values though, the physical-based two-grid BMIA/CAG method [30] is recommended; for even larger values, the Impedance Boundary Condition is more adapted. Moreover, the BMIA/CAG is efficient for surfaces with rms heights up to 2 or $3\lambda$ even more (up to $10\lambda$) with the multigrid BMIA/CAG method [31] and the Multilevel BMIA/CAG [29]. The efficiency decreases with larger values of $P$, because to reach the same precision, the number of terms in series (16) or (20) increases ($\mathcal{O}(P^2)$ number of terms).

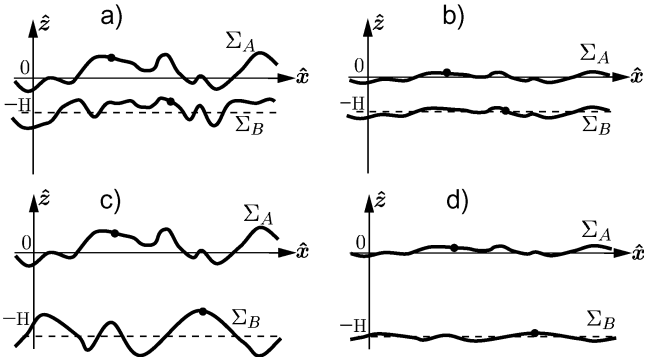


Fig. 4. Different configurations coped with a coupling of the kind BMIA/CAG. Case 1: (a) and (b), $H < 2$ or $3\lambda$. Case 2: (c), $H > 2$ or $3\lambda$ and $H \approx z_{d,\max}$. Case 3: (d), $H > 2$ or $3\lambda$ and $H \gg z_{d,\max}$.

## IV. Improvement of the Coupling Step With BMIA/CAG

Applying one of the fast methods quoted before speeds up the calculations $\left(\boldsymbol{Z}^A\right)^{-1}\cdot\boldsymbol{v}$ and $\left(\boldsymbol{Z}^B\right)^{-1}\cdot\boldsymbol{v}$ and reduces the complexity of both steps to $\mathcal{O}(N\log N)$. Accordingly, the most penalizing steps in the calculation of (9)

$$\boldsymbol{Y}_A^{(p)} = (\boldsymbol{Z}^A)^{-1}\cdot\boldsymbol{C}^{B\to A}\cdot(\boldsymbol{Z}^B)^{-1}\cdot\boldsymbol{C}^{A\to B}\cdot\boldsymbol{Y}_A^{(p-1)}$$

are now $\boldsymbol{C}^{B\to A}\cdot\boldsymbol{v}$ and $\boldsymbol{C}^{A\to B}\cdot\boldsymbol{v}$, each one having a complexity $\mathcal{O}(N^2)$. In this section, a method similar to BMIA/CAG is developed to reduce the complexity of these products.

At this point it is important to notice that the coupling between the surfaces $\Sigma_A$ and $\Sigma_B$ is the summation of the interactions between all the couples of points $(\boldsymbol{r}_m^A, \boldsymbol{r}_n^B)$ belonging, respectively, to $\Sigma_A$ and $\Sigma_B$. The interaction between two of these points can be seen as the interaction between two points of a same imaginary surface with an rms height of about $\sqrt{H^2 + \left(\sigma_h^A\right)^2 + \left(\sigma_h^B\right)^2}$. Hence, we can apply the multigrid BMIA/CAG method [31] or the multilevel BMIA/CAG method [29]. These methods were developed for surfaces with high rms heights (more than $3\lambda$). Nevertheless, because of their complexity (of programming and of operations) an adaptation of these methods for the coupling step would lead to an inefficient method for high values of $H$.

In the general case, developments similar to (16) and (20) can be obtained by adapting the BMIA/CAG. They are quite more complex for the coupling matrices; nevertheless, in some configurations, we can obtain some simple formulas, and interestingly in the case of big values of $H$. Actually, the main parameter that is discriminant in the choice of the algorithm is the mean thickness $H$ of the layer. In any case, the rms of heights of each interface is assumed to be less than $2\lambda$. All possible configurations are represented in Fig. 4.

### A. Case 1: $H < 2$ or $3\lambda$

When the mean thickness is less than 2 or $3\lambda$, a classical BMIA/CAG algorithm can be applied, as said previously, con-

sidering that the couple of points $(\boldsymbol{r}_m^A, \boldsymbol{r}_n^B)$ belongs to a same surface.

Let $x_d = x_m - x_n$ and $x_{d0} \gg \max_{n,m=1...N} |\zeta_m^A - \zeta_n^B|$; let $R_d = \lfloor x_{d0}/\Delta x \rfloor$. Then, let us consider for example the coupling sub-matrix $\boldsymbol{F}$ corresponding to the TE PC case; defining similarly as (11)

$$\boldsymbol{F} = \boldsymbol{F}^{(s)} + \boldsymbol{F}^{(w)} \tag{23}$$

we get the same decomposition for $\boldsymbol{F}^{(w)}$ as (16); the corresponding matrices $\boldsymbol{T}_q^{(\mathrm{pre})}$, $\boldsymbol{T}_{p,q}^{(\mathrm{post})}$ and $\boldsymbol{Z}_p^{(d)}$ are similar to (17), substituting $\zeta_n$ with $\zeta_n^B$ and $\zeta_m$ with $\zeta_m^A$.

The same method can easily be applied to the matrix $\boldsymbol{H}$ and also to the coupling matrices $\boldsymbol{E}$ and $\boldsymbol{G}$, using for the two latter the similarity with (22).

### B. $H > 2$ *or* $3\lambda$

To derive the BMIA/CAG method in this case, the distance $\|\boldsymbol{r}_n^A - \boldsymbol{r}_m^B\|$ (or similarly $\|\boldsymbol{r}_n^B - \boldsymbol{r}_m^A\|$) has to be approximated by a distance which is only dependent on $|x_d| = |x_m - x_n|$ for a given mean thickness $H$

$$\begin{aligned} \left\|\boldsymbol{r}_m^A - \boldsymbol{r}_n^B\right\|^2 &= (x_m - x_n)^2 + \left(\zeta_m^A - \zeta_n^B\right)^2 \\ &= x_d^2 + H^2 + 2Hz_d + z_d^2 \\ &= \left(x_d^2 + H^2\right)\left[1 + \frac{2Hz_d + z_d^2}{x_d^2 + H^2}\right] \\ \text{where} \quad z_d &= \zeta_m^A - \left(\zeta_n^B + H\right) = h_m^A - h_n^B. \end{aligned} \tag{24}$$

$h_m^A = \zeta_m^A$ and $h_n^B = \zeta_n^B + H$ are the elevation of the points $\boldsymbol{r}_m^A$ and $\boldsymbol{r}_n^B$ with respect to the mean lines $z = 0$ and $z = -H$, respectively, (Fig. 5), hence $h^A$ and $h^B$ are two Gaussian variables with zero mean value. Let us denote $z_{d,\max} = \max_{n,m=1...N}(|z_d|)$. Care must be taken at this point; the definition of $z_d$ is different from in the other sections. Furthermore, the distance which is only dependent on $|x_d|$ is the hypotenuse of the triangle $MM'M''$ (Fig. 5), with a length of $\|\boldsymbol{MM'}\| = \sqrt{x_d^2 + H^2}$. Let us choose $x_{d0}$ such that

$$x_{d0}^2 + H^2 \gg z_{d,\max}^2. \tag{25}$$

This condition ensures that $(2Hz_d + z_d^2)/(x_d^2 + H^2) \ll 1$ if $|x_d| > x_{d0}$. This is useful, when in (24), to derive an approximation for the Green function and its normal derivate, used in the coupling matrices $\boldsymbol{E}$, $\boldsymbol{F}$, $\boldsymbol{G}$ and $\boldsymbol{H}$. For example, we can approximate the term $g(\boldsymbol{r_m^A}, \boldsymbol{r_n^B})$, of $\boldsymbol{F}$, similarly to (13)

$$\begin{aligned} g\left(\boldsymbol{r_m^A}, \boldsymbol{r_n^B}\right) &= \frac{i}{4} H_0^{(1)}\left(k_1\sqrt{x_d^2 + H^2}\left[1 + \frac{2Hz_d + z_d^2}{x_d^2 + H^2}\right]^{1/2}\right) \\ &\approx \sum_{p=0}^{P} a_p\left(|x_d|\right)\left(2Hz_d + z_d^2\right)^p \end{aligned} \tag{26}$$

with

$$a_p\left(|x_d|\right) = \frac{i}{4}\frac{H_p^{(1)}\left(k_1\sqrt{x_d^2 + H^2}\right)}{p!}\left(\frac{-k_1}{2\sqrt{x_d^2 + H^2}}\right)^p. \tag{27}$$

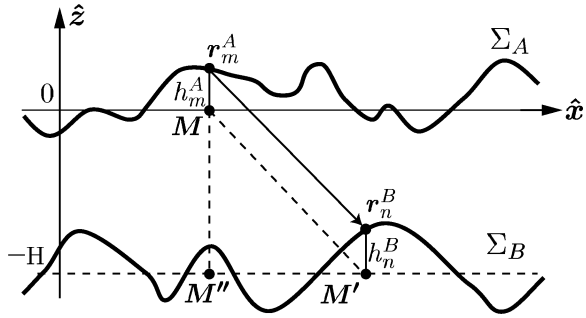


Fig. 5. Acceleration of coupling with BMIA/CAG. $\|\boldsymbol{r}_m^A - \boldsymbol{r}_n^B\|$ is approximated by $\|\boldsymbol{MM'}\|$.

In the same way, we obtain for the coupling matrix $\boldsymbol{E}$

$$\begin{aligned} &-\frac{\partial g\left(\boldsymbol{r}_m^A, \boldsymbol{r}_n^B\right)}{\partial n} \\ &= -\frac{ik}{4}\frac{H_0^{(1)}\left(k_1\left\|\boldsymbol{r}_m^A - \boldsymbol{r}_n^B\right\|\right)}{\left\|\boldsymbol{r}_m^A - \boldsymbol{r}_n^B\right\|}\alpha_{n,m} \\ &= \sum_{p=0}^{P} \underbrace{-\frac{ik}{4}\frac{H_{p+1}^{(1)}\left(k\sqrt{x_d^2 + H^2}\right)}{p!\sqrt{x_d^2 + H^2}}\left(\frac{-k}{2\sqrt{x_d^2 + H^2}}\right)^p}_{a_p(|x_d|)} \\ &\quad \times \left(2Hz_d + z_d^2\right)^p \alpha_{n,m} \end{aligned} \tag{28}$$

where

$$\alpha_{n,m} = \zeta_n^{B'}(x_n - x_m) - \left(\zeta_n^B - \zeta_m^A\right) \tag{29}$$

and $\zeta^{B'}$ denotes the derivative of $\zeta^B$.

*1) Case 2: $H > 2$ or $3\lambda$, and $H \approx z_{d,\max}$:* The detailed study of this case can be found in Appendix II.

*2) Case 3: $H > 2$ or $3\lambda$, and $H \gg z_{d,\max}$:* The limit case $H \gg z_{d,\max}$ leads to a simple result. In this case

$$2Hz_d + z_d^2 \approx 2Hz_d. \tag{30}$$

Then, considering for example the matrix $\boldsymbol{F}$, defining similarly as (11)

$$\boldsymbol{F} = \boldsymbol{F}^{(s)} + \boldsymbol{F}^{(w)} \tag{31}$$

and introducing (30) into (26), we get

$$\boldsymbol{F}^{(w)} = \sum_{p=0}^{P} \boldsymbol{Z}_p^{(w)} = \sum_{p=0}^{P}\sum_{q=0}^{p} \boldsymbol{T}_{p,q}^{(\mathrm{post})} \boldsymbol{Z}_p^{(d)} \boldsymbol{T}_q^{(\mathrm{pre})} \tag{32}$$

where $\boldsymbol{T}_q^{(\mathrm{pre})}$ and $\boldsymbol{T}_{p,q}^{(\mathrm{post})}$ are diagonal matrices, and where $\boldsymbol{Z}_p^{(d)}$ is a Toeplitz matrix. The elements are given by

$$\begin{aligned} \left(\boldsymbol{T}_q^{(\mathrm{pre})}\right)_{nn} &= \left(-h_n^B\right)^q = \left(-\zeta_n^B - H\right)^q \\ \left(\boldsymbol{T}_{p,q}^{(\mathrm{post})}\right)_{mm} &= C_p^q\left(h_m^A\right)^{p-q} = C_p^q\left(\zeta_m^A\right)^{p-q} \\ \left(\boldsymbol{Z}_p^{(d)}\right)_{mn} &= \begin{cases} (2H)^p \Delta x a_p \\ \quad \times \left(|x_m - x_n|\right) & \text{if } |m-n| \geq R_d \\ 0 & \text{if } |m-n| < R_d \end{cases} \end{aligned} \tag{33}$$

We get in the same way for the matrix $\boldsymbol{E}$ by introducing (30) into (28)

$$\boldsymbol{E}^{(w)} = \sum_{p=0}^{P}\sum_{q=0}^{p}\Big[\boldsymbol{T}_{p,q}^{(\mathrm{post1})}\boldsymbol{Z}_p^{(d)}\boldsymbol{T}_{p,q}^{(\mathrm{pre1})} + \boldsymbol{T}_{p,q}^{(\mathrm{post2})}\boldsymbol{Z}_p^{(d)}\boldsymbol{T}_{p,q}^{(\mathrm{pre2})} + \boldsymbol{T}_{p,q}^{(\mathrm{post3})}\boldsymbol{Z}_p^{(d)}\boldsymbol{T}_{p,q}^{(\mathrm{pre3})}\Big] \quad (34)$$

where $(\boldsymbol{T}_{p,q}^{(\mathrm{prei})})_{i=1,2,3}$ and $(\boldsymbol{T}_{p,q}^{(\mathrm{posti})})_{i=1,2,3}$ are diagonal matrices and $\boldsymbol{Z}_p^{(d)}$ is a full matrix. There is a difference between (16), (20), and (32), (34), respectively, in the fact that the upper limit of the inner sum is $p$ and not $2p$. The elements of $\bar{\boldsymbol{E}}^{(w)}$ are given by

$$\begin{aligned}
\left(\boldsymbol{T}_{q,r}^{(\mathrm{pre1})}\right)_{nn} &= \left(-\zeta_n^B - H\right)^q\left[\zeta_n^{B'}x_n - \zeta_n^B\right]\\
\left(\boldsymbol{T}_{q,r}^{(\mathrm{pre2})}\right)_{nn} &= \left(-\zeta_n^B - H\right)^q\zeta_n^{B'}\\
\left(\boldsymbol{T}_{q,r}^{(\mathrm{pre3})}\right)_{nn} &= \left(-\zeta_n^B - H\right)^q\\
\left(\boldsymbol{T}_{p,q,r}^{(\mathrm{post1})}\right)_{mm} &= C_p^q\left(\zeta_m^A\right)^{p-q}\\
\left(\boldsymbol{T}_{p,q,r}^{(\mathrm{post2})}\right)_{mm} &= -C_p^q\left(\zeta_m^A\right)^{p-q}.x_m\\
\left(\boldsymbol{T}_{p,q,r}^{(\mathrm{post3})}\right)_{mm} &= C_p^q\left(\zeta_m^A\right)^{p-q}\zeta_m^A\\
\left(\boldsymbol{Z}_p^{(d)}\right)_{mn} &= \begin{cases}(2H)^p\Delta x a_p \\ \quad\times\left(|x_m - x_n|\right) & \text{if } |m-n| \geq R_d\\ 0 & \text{if } |m-n| < R_d.\end{cases}
\end{aligned} \quad (35)$$

The other matrices $\boldsymbol{G}$ and $\boldsymbol{H}$ are also easily deduced from the expressions of case 2 (52) and (48), respectively.

As a conclusion, the complexity of the coupling step is then also $\mathcal{O}(N\log N)$, although some formulas are more complex in the coupling step than in the local interaction step. Nevertheless, it is worth noticing that for the calculation of

$$\boldsymbol{Y}_A^{(p)} = (\boldsymbol{Z}^A)^{-1}\cdot\boldsymbol{C}^{B\to A}\cdot(\boldsymbol{Z}^B)^{-1}\cdot\boldsymbol{C}^{A\to B}\cdot\boldsymbol{Y}_A^{(p-1)}$$

the products $\boldsymbol{C}^{A\to B}\cdot\boldsymbol{v}$ and $\boldsymbol{C}^{B\to A}\cdot\boldsymbol{v}$ are performed only once for each order of PILE method. On the opposite, the matrix-vector products $\boldsymbol{Z}^A\cdot\boldsymbol{v}$ and $\boldsymbol{Z}^B\cdot\boldsymbol{v}$ are performed many times in order to iteratively find $(\boldsymbol{Z}^A)^{-1}\cdot\boldsymbol{v}$ and $(\boldsymbol{Z}^B)^{-1}\cdot\boldsymbol{v}$.

As a conclusion, we call PILE-BMIA/CAG this method, in order to differentiate it from the PILE method, using only exact matrices inversions for the local interactions and exact matrix-vector products for the coupling step.

## V. Comparison With References Methods

The validity domain of the PILE method, relying on the condition $||\boldsymbol{M}_c|| < 1$ where the norm used is the spectral radius, has been studied in [16]. It is quite large, the only limitation being the poor convergence with very thin and very rough layers.

In this section the validity and the convergence of the PILE combined to the BMIA/CAG is investigated. Different configurations are considered, corresponding to case 1 ($H < 2$ or $3\lambda$), case 2 ($H > 2$ or $3\lambda$, and $H \approx z_{d,\max}$) and case 3 ($H > 2$ or $3\lambda$, and $H \gg z_{d,\max}$).

In order to find the good parameters to achieve a good convergence of PILE-BMIA/CAG for each configuration, we work in two steps: first, we look for the convergence of the exact PILE method, comparing it to the reference results provided by a direct inversion of the impedance matrix. More precisely, we seek the minimum order $P_{\mathrm{pile}}$ (8) of PILE method for which the mean absolute error over $\theta_s \in [-90°; 90°]$ on the bistatic scattering coefficient (BSC) is less than 0.1 dB; this order, $P_{\mathrm{pile}}$, corresponds to the number of prevailing reflections inside the layer.

Second, launching the PILE-BMIA/CAG at order $P_{\mathrm{pile}}$, we look for an acceptable order of truncation $P$ of the series of the coupling step, following the same procedure as before (error less than 0.1 dB on the BSC).

Besides, we compare the PILE-BMIA/CAG to the forward-backward (FB) method developed for a layer by Moss *et al.* [18]. Actually, in his article, Moss speeds up the FB method with the Novel Spectral Acceleration [36], as we did using the BMIA/CAG for the PILE. The FBNSA method is faster than PILE-BMIA/CAG, with a complexity of only $\mathcal{O}(N)$ versus $\mathcal{O}(N\log N)$. Nevertheless, the two methods rely on different physical interpretations, and thus the validity domains are *a priori* different. That is why, even if the direct comparison of the PILE-BMIA/CAG to the FB-NSA is beyond the scope of this paper, it seems interesting to compare PILE method to FB.

In all the configurations the lower medium $\Omega_2$ is perfectly conducting (case (c) of Fig. 2), and the relative permittivity of the inner medium $\Omega_1$ is $\varepsilon_{r,1} = 2 + 0.01i$. The corresponding skin depth $\delta$ is quite large: $\delta \simeq 45\lambda$. It is worth noticing that if the losses are lower, the total length $L$ of the interfaces have to be increased to avoid edge effects. Each interface, of total length $L = 50\lambda$ and with rms slopes $\sigma_p^{A,B} = \{0.2, 0.2\}$, is sampled at $\Delta x = \lambda/10$; the surface height spectrum is Gaussian. The illuminating beam is a Thorsos beam of attenuation parameter $g = L/10$, and an incidence angle of $\theta_i = 0°$.

### A. Configuration of Case 1

First we study a configuration where the two interfaces fulfill the conditions of applicability of the small perturbation method: rms heights $\sigma_h^A = \sigma_h^B = 0.05\lambda$, rms slopes $\sigma_p^A = \sigma_p^B = 0.2$. The mean thickness $H = 0.5\lambda$ is less than $2\lambda$ (case 1 given in Section IV-A).

The convergence of the exact PILE method is studied in the TE polarization in Fig. 6 and Fig. 7. By exact, we mean that each term of the product

$$\boldsymbol{Y}_A^{(p)} = (\boldsymbol{Z}^A)^{-1}\cdot\boldsymbol{C}^{B\to A}\cdot(\boldsymbol{Z}^B)^{-1}\cdot\boldsymbol{C}^{A\to B}\cdot\boldsymbol{Y}_A^{(p-1)}$$

is computed rigorously, using exact matrix-inversions and exact matrix-products. The reference BSC in these figures is obtained using an exact inversion of the impedance matrix of the whole layer $\boldsymbol{Z}$. The BSC obtained in TM polarization, very similar, is not plotted here. From Fig. 7, PILE method converges rapidly, and the BSC at order 15 is very close to the reference BSC; FB BSC is not plotted because the method did not converge.

The mean error between the exact BSC and the PILE BSC is shown for both polarizations on Fig. 8. The error for the FB is also given. The trends in TE and TM for PILE are the same, and also similar to the FB in TM. The FB in the TE polarization

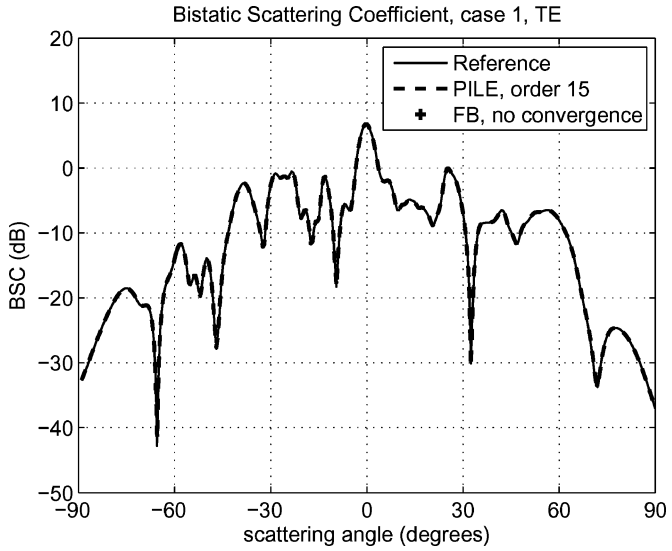


Fig. 6. Case 1. BSC plotted in a dB scale. Comparison of the BSC obtained exactly (Reference), with exact PILE, and with FB. The parameters of the problem are: $\sigma_h^A = \sigma_h^B = 0.05\lambda$, $\sigma_p^A = \sigma_p^B = 0.2$; $H = 0.5\lambda$, $\varepsilon_{r,1} = 2 + 0.01i$, $\theta_i = 0°$. TE polarization.

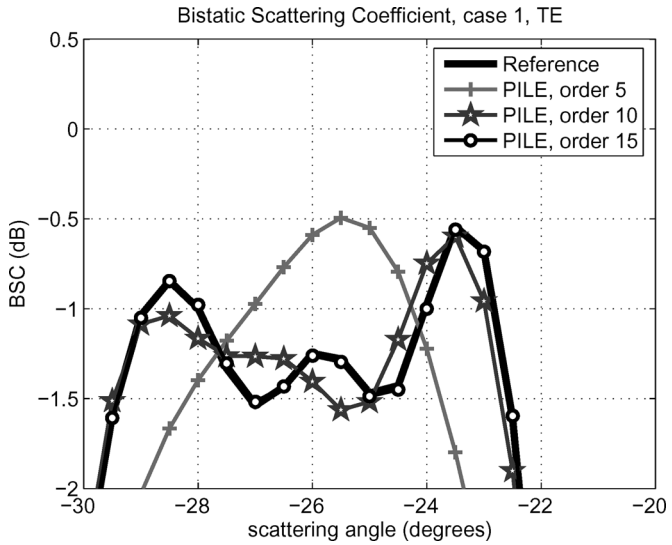


Fig. 7. Case 1. BSC plotted in a dB scale. Comparison of the BSC obtained exactly (Reference) and with exact PILE, at different orders. Zoom of Fig. 6.

does not converge, even for a higher order of FB (not represented here); this implies that the FBNSA in TE does not converge either for this configuration. Concerning the BSC, the mean error is less than 0.1 dB for PILE orders greater than $P_{\text{pile}} = 15$ in TE and TM polarizations.

To choose now the parameters of the BMIA/CAG, the [21], [27] are interesting. As a rule of thumb, for each interface $x_{d0} \simeq 10\sigma_h$ so $R_d \simeq \lfloor 10\sigma_h/\Delta x \rfloor$; actually we keep the bandwidth $R_d > 50$ in all simulations to get a satisfactory precision; moreover, an order of truncation of $P = 5$ or 6 is enough for rms heights up to $\sigma_h = 0.5\lambda$. Besides, in case 1, the coupling step is based on the classical formulas of the BMIA/CAG for a single surface, so the corresponding parameters can be found assuming that the virtual surface has an rms height of about

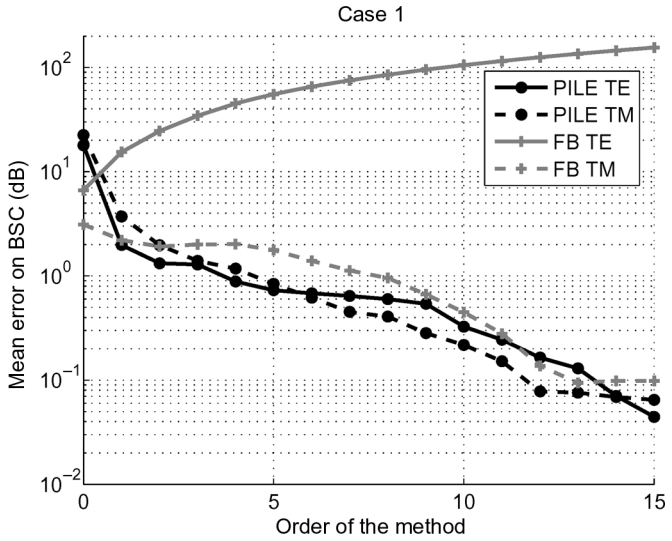


Fig. 8. Case 1. Mean error (in decibels) between the BSC obtained from an exact inversion and the exact PILE. A comparison with the exact FB method is also shown. TE and TM polarizations. Each order of PILE method corresponds to a downward-upward propagation and for FB method, to a FB (right-left) propagation.

$\sigma_{h,layer}^{eq} \simeq \sqrt{H^2 + (\sigma_h^A)^2 + (\sigma_h^B)^2}$; with the given parameters, $\sigma_{h,layer}^{eq} \simeq 0.51\lambda$.

Finally, for the simulations of case 1 we chose: $R_d^A = R_d^B = 50$ coefficients, the orders of truncation $P^A = P^B = 6$ for the upper and lower interfaces, and for the coupling $R_d^{\text{coupl}} \simeq \lfloor 10\sigma_{h,\text{layer}}^{eq}/\Delta x \rfloor = 60$, and $P = 10$. With these parameters, the BSC calculated at different orders with the PILE-BMIA/CAG is very close to the one calculated with the exact PILE; even the mean error in dB is indistinguishable. The results are hence not shown here.

### *B. Configuration of Case 2*

Hereafter we study a configuration where the two interfaces fulfills the conditions of application of the geometrical optics approximation: rms heights $\sigma_h^A = \sigma_h^B = 0.5\lambda$, rms slopes $\sigma_p^A = \sigma_p^B = 0.2$. The mean thickness $H = 5\lambda$, is bigger than $2\lambda$ and $z_{d,\max} = \max_{n,m=1\ldots N}(|\zeta_m^A - (\zeta_n^B + H)|) \simeq 2\lambda$ so $H$ and $z_{d,\max}$ have the same order of magnitude. In this case, we have to use the formulas of case 2, that is (47), (48), (51) and (52).

First, the convergence of the exact PILE method is studied in the TE polarization in Fig. 9. The BSC obtained in TM polarization, very similar, is not plotted here. FB method converges and its BSC appears to be in very good agreement with the others.

Fig. 10 shows the mean error between the exact BSC and the PILE BSC for both polarizations. The BSC for orders $P_{\text{pile}} > 4$ is in very good agreement with the reference BSC, with a mean error less than 0.1 dB. The BSC provided by PILE converges faster than in the former configuration. This can be explained physically: as the thickness $H$ is increased (from $0.5\lambda$ to $5\lambda$), the number of reflections inside the layer that contributes significantly to the total BSC decreases. As a last remark, the rate of convergence of FB is twice slower than for PILE method, in both configurations.

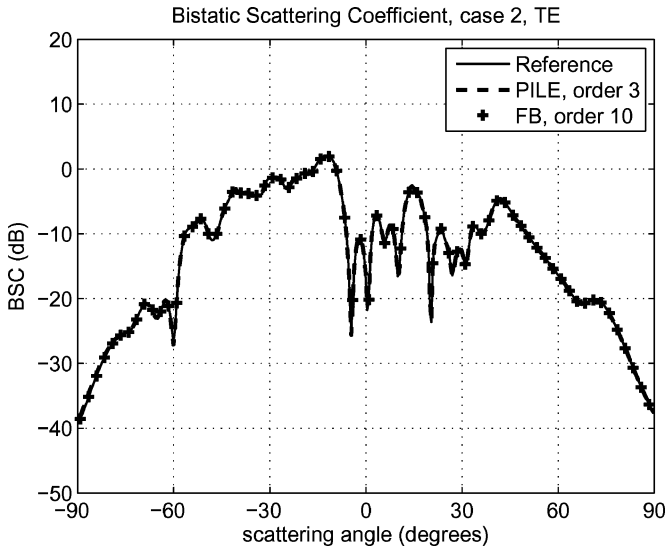


Fig. 9. Case 2. BSC plotted in a dB scale. Comparison of the BSC obtained exactly (Reference) and by exact PILE, at different orders. The parameters are: $\sigma_h^A = \sigma_h^B = 0.5\lambda$, $\sigma_p^A = \sigma_p^B = 0.2$; $H = 5\lambda$, $\varepsilon_{r,1} = 2 + 0.01i$, $\theta_i = 0°$. TE polarization.

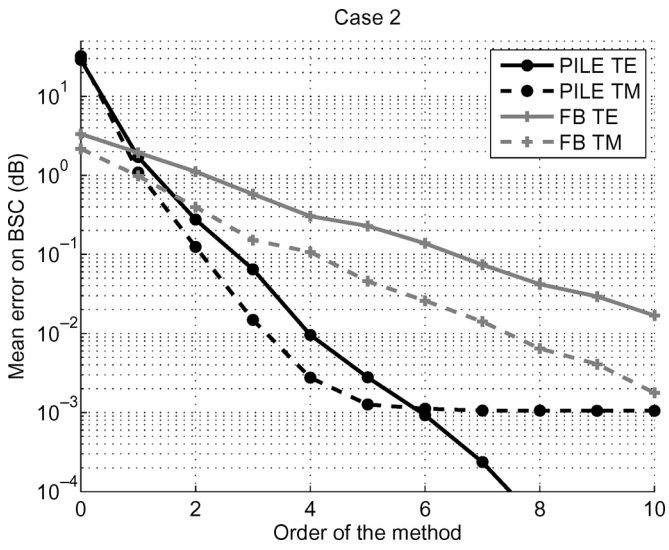


Fig. 10. Case 2. Mean error (in decibels) between the bistatic scattering coefficient (BSC) obtained from an exact inversion and the exact PILE. The mean error is plotted in a semilog-scale. TE and TM polarizations.

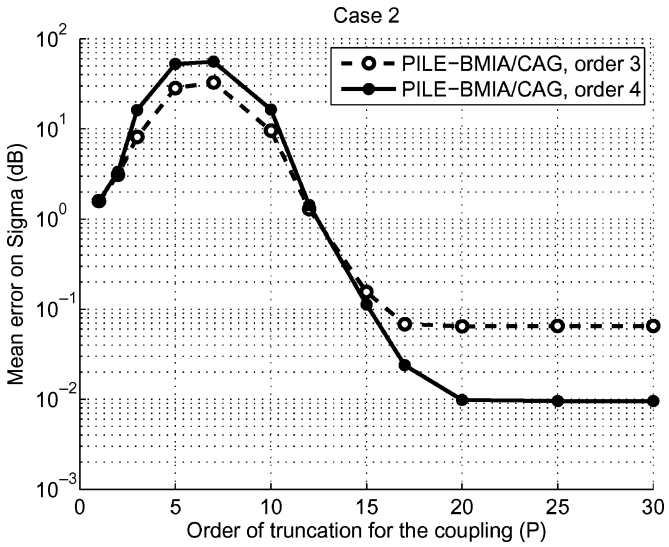


Fig. 11. Case 2. Mean error (in decibels) for the PILE-BMIA/CAG versus the order of truncation $P$ of the series involved in the coupling step. PILE at order 3 and 4. TE polarization.

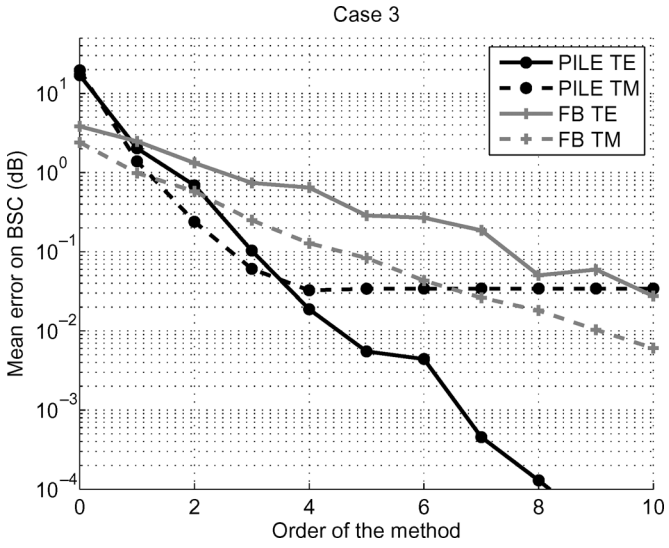


Fig. 12. Case 3. Mean error (in decibels) between the BSC obtained from an exact inversion and the exact PILE. The parameters are: $\sigma_h^A = \sigma_h^B = 0.05\lambda$, $\sigma_p^A = \sigma_p^B = 0.2$; $H = 5\lambda$, $\varepsilon_{r,1} = 2 + 0.01i$, $\theta_i = 0°$. TE and TM polarizations.

In a second step, we seek the values of the parameters of the BMIA/CAG combined to PILE method. The parameters of the BMIA/CAG for the local interactions are calculated using the same rule of thumb as in the previous configuration: $R_d^{A,B} \simeq \lfloor 10\sigma_h^{A,B}/\Delta x \rfloor = 50$; the chosen orders of truncation for the upper and lower interfaces are $P^A = P^B = 10$. For the coupling interactions, let choose the limit interaction distance $x_{d0}$ such that $x_{d0}^2 + H^2 \gg z_{d,\max}^2 \simeq 4\lambda^2$, hence for example $x_{d0} = 5\lambda$ and then $R_d^{\text{coupl}} = 50$. To find the last parameter, the order of truncation $P$ of the series in the coupling formulas (50) and (46), we plot in Fig. 11 the mean error on the BSC versus this parameter, for $P_{\text{pile}} = 3$ and 4. Only the TE polarization is represented here, the TM being very similar.

Fig. 11 shows how PILE-BMIA/CAG is as precise as exact PILE once the correct parameters are chosen for the BMIA/CAG. From Fig. 10, the mean error for the exact PILE is 0.7 dB and 0.01 dB for $P_{\text{pile}} = 3$ and 4, respectively. A same level of precision is reached in Fig. 11 for $P > 20$.

### C. Configuration of Case 3

Third, the purpose is to study a configuration leading to the validity domain of case 3. Selecting $\sigma_h^A = \sigma_h^B = 0.05\lambda$, and rms slopes $\sigma_p^A = \sigma_p^B = 0.2$, and $H = 5\lambda$, we get $H \gg z_{d,\max} \simeq 0.23\lambda$. In this case, we have to use the formulas of case 3, that is (33) and (35).

Fig. 12 plots the convergence of the exact PILE and the FB method. Exact PILE method reaches the precision 0.1 dB and less for $P_{\text{pile}} > 3$. In this configuration, the rate of decrease of

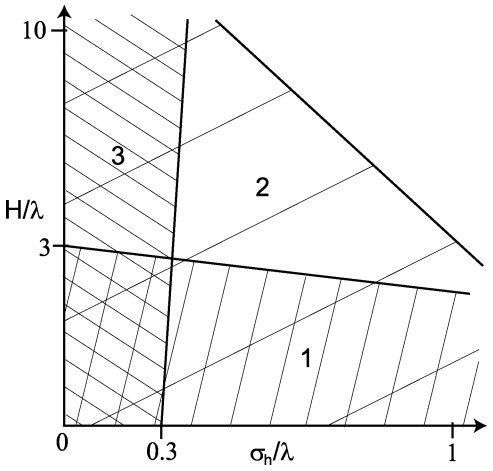


Fig. 13. Domain of convergence of PILE-BMIA/CAG corresponding to an error in the BSC less than 0.1 dB for the following set of parameters: $P_{\text{pile}}$ less than 20, orders of truncation $P^A = P^B = 6$ and $P = 20$ for the coupling; for the bandwidth, $R_d^{A,B} = R_d^{\text{coupl}} = 100$ coefficients. Both surfaces are equal; $\sigma_h = \sigma_h^{A,B}$ and $\sigma_p^{A,B} = 0.2$. $\theta_i = 0°$. $L = 50\lambda$. Formulas of domain 1: cf Section IV-A; domain 2: cf Section IV-B-1; domain 3: cf Section IV-B-2.

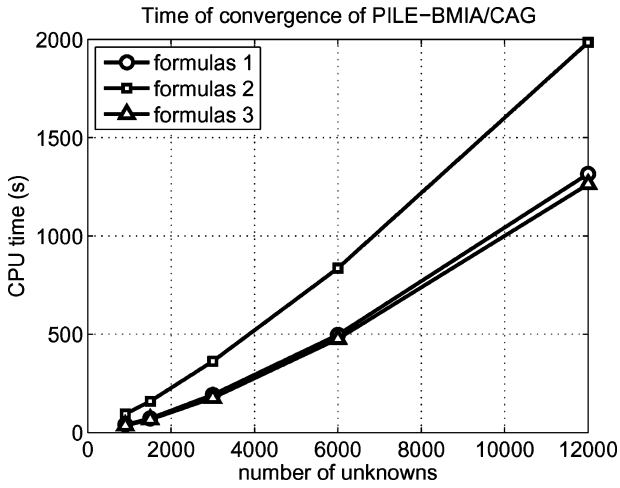


Fig. 14. CPU time of convergence of PILE-BMIA/CAG for the following set of parameters: $P_{\text{pile}} = 5$, orders of truncation $P^A = P^B = 6$ and $P = 20$ for the coupling; $R_d^{A,B} = R_d^{\text{coupl}} = 100$ coefficients. Formulas 1: cf Section IV-A; formulas 2: cf Section IV-B-1; formulas 3: cf Section IV-B-2.

the FB is lower than for PILE; nevertheless, in the TM case, the error of PILE method does not decrease below 0.03 dB at orders 4 and higher whereas the FB method reaches a better precision than PILE for orders 7 and up.

The order of truncation $P$ of the coupling step is chosen as in Section V-B studying the mean error on the BSC as a function of $P$. The convergence is faster than for case 2, probably because the rms heights of the interfaces are lower. Actually, for the parameters $P^A = P^B = 10$ and $R_d^{A,B} = R_d^{\text{coupl}} = 50$, we found that for $P > 4$ the precision of PILE-BMIA/CAG is excellent.

### *D. Validity Domain and Computation Time*

All three previous configurations have been chosen to fit a particular case studied in Section IV. From a practical point of view, one has to pick the right formula and the right parameters to fit a given configuration. Hereafter a way to make a first guess automatically is proposed. For this purpose we consider a given set of parameters and study the convergence of PILE-BMIA/CAG as a function of $\sigma_h = \sigma_h^{A,B}$ and $H$ (the surfaces are supposed equal and translated from each other). The three formulas are used and convergence is established when a mean error of 0.1 dB or less is reached for an order $P_{\text{pile}}$ less than 20. The fixed parameters are $P^A = P^B = 6$, $P^{\text{coupl}} = 20$ and $R_d^{A,B} = R_d^{\text{coupl}} = 100$. For the incident beam $\theta_i = 0°$ and $g = L/10$; the polarization has little effect on the convergence. The surfaces have a total length $L = 50\lambda$, rms slopes $\sigma_p^{A,B} = \{0.2, 0.2\}$, and $\Delta x = \lambda/10$; the relative permittivity of the inner medium is $\varepsilon_{r,1} = 2 + 0.01i$. The convergence domain is shown in Fig. 13. Some domains are overlaid, and in this case, any formula can be used. Formulas of cases 1 and 3 are always faster than the ones of case 2, but the latter ones are more universal than the others. However, let us recall that the PILE method is less accurate for very thin layers. Finally, in order to get an efficient method with a minimum $P_{\text{pile}}$ order, the residual error can be considered. As a rule of thumb, for $H > 1\lambda$, $P_{\text{pile}} < 10$ is enough.

The CPU time of the PILE-BMIA/CAG method is shown in Fig. 14, where the same parameters are used, and the order $P_{\text{pile}} = 5$ is constant. The number of unknowns is equal to $3N$ where $N$ is the number of samples per interface, considering the layered PC case (Fig. 2). A 3 GHz personal computer with 2 GB of RAM is used in this work. We can verify from a linear regression that the complexity of the PILE-BMIA/CAG is $\mathcal{O}(N \log N)$.

## VI. Conclusion

In this paper, we presented a new efficient method to predict the field scattered from a 1-D stack of two rough interfaces. The method is based on the rigorous PILE method [16], and it was accelerated using the fast method BMIA/CAG. The BMIA/CAG for a single-interface was first reminded and cast in a very simple and convenient way. Then the BMIA/CAG was adapted to take into account the coupling between the two interfaces, and different formulas where given for three different kinds of configurations. The resulting method, the PILE-BMIA/CAG, has a complexity of only $\mathcal{O}(N \log N)$.

Then a numerical validation of the PILE-BMIA/CAG was undertaken comparing it to a reference method, and to the recent FB for a layer [18].

The convergence of PILE-BMIA/CAG has been established for layers with a thickness of $10\lambda$ and more; in some cases the PILE method converged whereas the FB method did not. Nevertheless this may be not a general rule; a more comprehensive study should be carried out to explore the convergence properties of both methods. At this point, we can only note that the underlying physical interpretation of the PILE method is different from for the FB method [18], and the validity domains are thus also different.

In conclusion, even if the PILE-BMIA/CAG is not the fastest rigorous method available (as the FBNSA [18] for example), it has in return a large validity domain, that makes it quite robust. Furthermore, for some configurations, simpler formulas can be used that reduced the computation time.

## APPENDIX I
## BLOCK-MATRICES OF THE GLOBAL IMPEDANCE MATRIX $\boldsymbol{Z}$

For the dielectric case, the block-matrices $\boldsymbol{A}^A$, $\boldsymbol{B}^A$, $\boldsymbol{C}^A$, $\boldsymbol{D}^A$, $\boldsymbol{E}$, $\boldsymbol{F}$, $\boldsymbol{G}$ and $\boldsymbol{H}$ of the impedance matrix $\boldsymbol{Z}$ have the following expressions:

$$\boldsymbol{Z}=\begin{bmatrix} \boldsymbol{Z}^A & \boldsymbol{C}^{B\to A} \\ \boldsymbol{C}^{A\to B} & \boldsymbol{Z}^B \end{bmatrix}=\begin{bmatrix} \boldsymbol{A}^A & \boldsymbol{B}^A & \boldsymbol{0} & \boldsymbol{0} \\ \boldsymbol{C}^A & \rho_{10}\boldsymbol{D}^A & \boldsymbol{E} & \boldsymbol{F} \\ \boldsymbol{G} & \rho_{10}\boldsymbol{H} & \boldsymbol{A}^B & \boldsymbol{B}^B \\ \boldsymbol{0} & \boldsymbol{0} & \boldsymbol{C}^B & \rho_{21}\boldsymbol{D}^B \end{bmatrix}. \tag{36}$$

In the following expressions, $k_i$ stands for the wave number of the medium $\Omega_i$, and $\rho_{ij}=\epsilon_i/\epsilon_j$ where $\epsilon_i$ is the permittivity of the medium $\Omega_i$. $\Sigma_A$ and $\Sigma_B$ are the upper and lower surfaces, respectively

$$A^A_{mn}=\begin{cases} -\frac{i\triangle x k_0}{4}\frac{H_1^{(1)}\left(k_0\left\|\boldsymbol{r}_n^A-\boldsymbol{r}_m^A\right\|\right)}{\left\|\boldsymbol{r}_n^A-\boldsymbol{r}_m^A\right\|} \\ \quad\times\left\{\zeta_n^{A'}\cdot(x_n-x_m)-\left(\zeta_n^A-\zeta_m^A\right)\right\} & \text{for } m\neq n \\ +\frac{1}{2}-\frac{\triangle x}{4\pi}\frac{\zeta^{A''}(x_m)}{1+\left(\zeta^{A'}(x_m)\right)^2} & \text{for } m=n \end{cases} \tag{37}$$

with $\zeta_n^A=\zeta^A(x_n)$ and $\zeta_n^{A'}=\zeta^{A'}(x_n)$ and $\zeta_m^{A''}=\zeta^{A''}(x_m)$

$$B^A_{mn}=\begin{cases} \gamma_n^A\frac{i\triangle x}{4}H_0^{(1)}\left(k_0\left\|\boldsymbol{r}_n^A-\boldsymbol{r}_m^A\right\|\right) & \text{for } m\neq n \\ \gamma_n^A\frac{i\triangle x}{4}\left[1+i\frac{2}{\pi}\log\left(\frac{e^\gamma}{2}\frac{k_0\triangle x}{2e}\gamma_n^A\right)\right] & \text{for } m=n \end{cases} \tag{38}$$

$$C^A_{mn}=\begin{cases} -\frac{i\triangle x k_1}{4}\frac{H_1^{(1)}\left(k_1\left\|\boldsymbol{r}_n^A-\boldsymbol{r}_m^A\right\|\right)}{\left\|\boldsymbol{r}_n^A-\boldsymbol{r}_m^A\right\|} \\ \quad\times\left\{\zeta_n^{A'}\cdot(x_n-x_m)-\left(\zeta_n^A-\zeta_m^A\right)\right\} & \text{for } m\neq n \\ -\frac{1}{2}-\frac{\triangle x}{4\pi}\frac{\zeta^{A''}(x_m)}{1+\left(\zeta^{A'}(x_m)\right)^2} & \text{for } m=n \end{cases} \tag{39}$$

$$D^A_{mn}=\begin{cases} \gamma_n^A\frac{i\triangle x}{4}H_0^{(1)}\left(k_1\left\|\boldsymbol{r}_n^A-\boldsymbol{r}_m^A\right\|\right) & \text{for } m\neq n \\ \gamma_n^A\frac{i\triangle x}{4} \\ \quad\times\left[1+i\frac{2}{\pi}\log\left(\frac{e^\gamma}{2}\frac{k_1\triangle x}{2e}\gamma_n^A\right)\right] & \text{for } m=n \end{cases} \tag{40}$$

$$E_{mn}=\left\{+\frac{i\triangle x k_1}{4}\frac{H_1^{(1)}\left(k_1\left\|\boldsymbol{r}_n^B-\boldsymbol{r}_m^A\right\|\right)}{\left\|\boldsymbol{r}_n^B-\boldsymbol{r}_m^A\right\|}\right. \\ \left.\times\left\{\zeta_n^{B'}\cdot(x_n-x_m)-\left(\zeta_n^B-\zeta_m^A\right)\right\}\right\}\forall\, m,n \tag{41}$$

$$F_{mn}=-\gamma_n^B\frac{i\triangle x}{4}H_0^{(1)}\left(k_1\left\|\boldsymbol{r}_m^A-\boldsymbol{r}_n^B\right\|\right)\quad\forall\, m,n \tag{42}$$

$$G_{mn}=\left\{+\frac{i\triangle x k_1}{4}\frac{H_1^{(1)}\left(k_1\left\|\boldsymbol{r}_n^A-\boldsymbol{r}_m^B\right\|\right)}{\left\|\boldsymbol{r}_n^A-\boldsymbol{r}_m^B\right\|}\right. \\ \left.\times\left\{\zeta_n^{A'}\cdot(x_n-x_m)-\left(\zeta_n^A-\zeta_m^B\right)\right\}\right\}\forall\, m,n \tag{43}$$

$$H_{mn}=-\gamma_n^A\frac{i\triangle x}{4}H_0^{(1)}\left(k_1\left\|\boldsymbol{r}_m^B-\boldsymbol{r}_n^A\right\|\right)\quad\forall\, m,n \tag{44}$$

with $\left\|\boldsymbol{r}_n^{A,B}-\boldsymbol{r}_m^{A,B}\right\|=\sqrt{(x_n-x_m)^2-\left(\zeta_n^{A,B}-\zeta_m^{A,B}\right)^2}$ and $\gamma_n^{A,B}=\sqrt{1+\left(\zeta_n^{A,B'}\right)^2}$; the superscript $\cdot'$ stands for the derivative; $\gamma\simeq 0.5772$ is Euler's constant $\boldsymbol{A}^B$, $\boldsymbol{B}^B$, $\boldsymbol{C}^B$ and $\boldsymbol{D}^B$ are very similar to $\boldsymbol{A}^A$, $\boldsymbol{B}^A$, $\boldsymbol{C}^A$ and $\boldsymbol{D}^A$, respectively, where $\boldsymbol{r}_{m,n}^A$ is replaced by $\boldsymbol{r}_{m,n}^B$, $\gamma_n^A$ by $\gamma_n^B$, $\zeta^A$ by $\zeta^B$, $k_0$ by $k_1$ and $k_1$ by $k_2$. These expressions can also be used in the perfectly conducting case.

## APPENDIX II
## CASE 2: $H>2$ OR $3\lambda$, AND $H\approx z_{d,\max}$

When $H\approx z_{d,\max}$, no approximation can be done over $(2Hz_d+z_d^2)^p$ in (26) and $(2Hz_d+z_d^2)^p\alpha_{n,m}$ in (28), so they have to be expanded rigorously.

Let us consider first the elements of $\boldsymbol{F}$ (26)

$$\begin{aligned}(z_d)^p(2H+z_d)^p&=\left[\sum_{q=0}^{p}C_p^q\left(h_m^A\right)^{p-q}\left(-h_n^B\right)^q\right] \\ &\quad\times\left[\sum_{r=0}^{p}C_p^r\left(2H+h_m^A\right)^{p-r}\left(-h_n^B\right)^r\right] \\ &=\sum_{q=0}^{p}\sum_{r=0}^{p}C_p^qC_p^r\left(h_m^A\right)^{p-q}\left(2H+h_m^A\right)^{p-r} \\ &\quad\times\left(-h_n^B\right)^{q+r}.\end{aligned} \tag{45}$$

Consequently, introducing (27) and (45) into (26), the impedance matrix of the weak interactions $\boldsymbol{F}^{(\boldsymbol{w})}$ defined by (23) can be written as:

$$\boldsymbol{F}^{(w)}=\sum_{p=0}^{P}\boldsymbol{Z}_p^{(w)}=\sum_{p=0}^{P}\sum_{q=0}^{p}\sum_{r=0}^{p}\boldsymbol{T}^{(\mathrm{post})}_{p,q,r}\boldsymbol{Z}_p^{(d)}\boldsymbol{T}^{(\mathrm{pre})}_{q,r} \tag{46}$$

where $\boldsymbol{T}^{(\mathrm{pre})}_{q,r}$ and $\boldsymbol{T}^{(\mathrm{post})}_{p,q,r}$ are diagonal matrices, and $\boldsymbol{Z}_p^{(d)}$ is a Toeplitz matrix. Substituting $h_m^A$ with $\zeta_m^A$ and $h_n^B$ with $\zeta_n^B+H$ into (45) we get

$$\begin{aligned}\left(\boldsymbol{T}^{(\mathrm{pre})}_{q,r}\right)_{nn}&=\left(-\zeta_n^B-H\right)^{q+r} \\ \left(\boldsymbol{T}^{(\mathrm{post})}_{p,q,r}\right)_{mm}&=C_p^qC_p^r\left(\zeta_m^A\right)^{p-q}\left(2H+\zeta_m^A\right)^{p-r} \\ \left(\boldsymbol{Z}_p^{(d)}\right)_{mn}&=\begin{cases}\Delta x a_p\left(|x_m-x_n|\right) & \text{if } |m-n|\geq R_d \\ 0 & \text{if } |m-n|<R_d\end{cases}\end{aligned} \tag{47}$$

where $a_p$ is given in (27).

The elements of $\boldsymbol{H}^{(\boldsymbol{w})}$ are obtained by substituting in (24) $\boldsymbol{r}_m^A$ and $\boldsymbol{r}_n^B$ by $\boldsymbol{r}_m^B$ and $\boldsymbol{r}_n^A$, respectively. Hence, $\boldsymbol{H}^{(\boldsymbol{w})}$ can be expanded as (46), with the following expressions for the matrices:

$$\begin{aligned}\left(\boldsymbol{T}^{(\mathrm{pre})}_{q,r}\right)_{nn}&=\left(\zeta_n^A\right)^{q+r} \\ \left(\boldsymbol{T}^{(\mathrm{post})}_{p,q,r}\right)_{mm}&=C_p^qC_p^r\left(-\zeta_m^B-H\right)^{p-q}\left(H-\zeta_m^B\right)^{p-r} \\ \left(\boldsymbol{Z}_p^{(d)}\right)_{mn}&=\begin{cases}\Delta x a_p\left(|x_m-x_n|\right) & \text{if } |m-n|\geq R_d \\ 0 & \text{if } |m-n|<R_d\end{cases}\end{aligned} \tag{48}$$

where $a_p$ is given in (27).

Let us consider now the elements of $\boldsymbol{E}$ matrix (28), and let us make a variable change in $\alpha_{n,m}$ (29), introducing $h^A$ and $h^B$. By definition of $h^B$, we have for the derivatives $\zeta^{B'}=h^{B'}$, so

$$\alpha_{n,m}=\left[h_n^{B'}(x_n-x_m)-\left(h_n^B-h_m^A-H\right)\right]$$

and then

$$(z_d)^p(2H+z_d)^p\alpha_{n,m}=\sum_{q=0}^{p}\sum_{r=0}^{p}C_p^qC_p^r\left(h_m^A\right)^{p-q}\times\left(2H+h_m^A\right)^{p-r}\left(-h_n^B\right)^{q+r}\alpha_{n,m}. \quad (49)$$

Thus

$$\boldsymbol{E}^{(w)}=\sum_{p=0}^{P}\sum_{q=0}^{p}\sum_{r=0}^{p}\left[\boldsymbol{T}_{p,q,r}^{(\mathrm{post1})}\boldsymbol{Z}_p^{(d)}\boldsymbol{T}_{q,r}^{(\mathrm{pre1})}+\boldsymbol{T}_{p,q,r}^{(\mathrm{post2})}\boldsymbol{Z}_p^{(d)}\boldsymbol{T}_{q,r}^{(\mathrm{pre2})}+\boldsymbol{T}_{p,q,r}^{(\mathrm{post3})}\boldsymbol{Z}_p^{(d)}\boldsymbol{T}_{q,r}^{(\mathrm{pre3})}\right] \quad (50)$$

with

$$\begin{aligned}
\left(\boldsymbol{T}_{q,r}^{(\mathrm{pre1})}\right)_{nn}&=\left(-\zeta_n^B-H\right)^{q+r}\left[\zeta_n^{B'}x_n-\zeta_n^B\right]\\
\left(\boldsymbol{T}_{q,r}^{(\mathrm{pre2})}\right)_{nn}&=\left(-\zeta_n^B-H\right)^{q+r}\zeta_n^{B'}\\
\left(\boldsymbol{T}_{q,r}^{(\mathrm{pre3})}\right)_{nn}&=\left(-\zeta_n^B-H\right)^{q+r}\\
\left(\boldsymbol{T}_{p,q,r}^{(\mathrm{post1})}\right)_{mm}&=C_p^qC_p^r\left(\zeta_m^A\right)^{p-q}\left(2H+\zeta_m^A\right)^{p-r}\\
\left(\boldsymbol{T}_{p,q,r}^{(\mathrm{post2})}\right)_{mm}&=-C_p^qC_p^r\left(\zeta_m^A\right)^{p-q}\left(2H+\zeta_m^A\right)^{p-r}x_m\\
\left(\boldsymbol{T}_{p,q,r}^{(\mathrm{post3})}\right)_{mm}&=C_p^qC_p^r\left(\zeta_m^A\right)^{p-q}\left(2H+\zeta_m^A\right)^{p-r}\zeta_m^A\\
\left(\boldsymbol{Z}_p^{(d)}\right)_{mn}&=\begin{cases}\Delta x a_p\left(|x_m-x_n|\right) & \text{if } |m-n|\geq R_d\\ 0 & \text{if } |m-n|<R_d\end{cases}.
\end{aligned} \quad (51)$$

where the coefficients $a_p$ are given in (28).

In a similar way, the elements of $\boldsymbol{G}^{(\boldsymbol{w})}$ are given by

$$\begin{aligned}
\left(\boldsymbol{T}_{q,r}^{(\mathrm{pre1})}\right)_{nn}&=\left(\zeta_n^A\right)^{q+r}\left[\zeta_n^{A'}x_n-\zeta_n^A\right]\\
\left(\boldsymbol{T}_{q,r}^{(\mathrm{pre2})}\right)_{nn}&=\left(\zeta_n^A\right)^{q+r}\zeta_n^{A'}\\
\left(\boldsymbol{T}_{q,r}^{(\mathrm{pre3})}\right)_{nn}&=\left(\zeta_n^A\right)^{q+r}\\
\left(\boldsymbol{T}_{p,q,r}^{(\mathrm{post1})}\right)_{mm}&=C_p^qC_p^r\left(-\zeta_m^B-H\right)^{p-q}\left(H-\zeta_m^B\right)^{p-r}\\
\left(\boldsymbol{T}_{p,q,r}^{(\mathrm{post2})}\right)_{mm}&=-C_p^qC_p^r\left(-\zeta_m^B-H\right)^{p-q}\left(H-\zeta_m^B\right)^{p-r}x_m\\
\left(\boldsymbol{T}_{p,q,r}^{(\mathrm{post3})}\right)_{mm}&=C_p^qC_p^r\left(-\zeta_m^B-H\right)^{p-q}\left(H-\zeta_m^B\right)^{p-r}\zeta_m^B\\
\left(\boldsymbol{Z}_p^{(d)}\right)_{mn}&=\begin{cases}\Delta x a_p\left(|x_m-x_n|\right) & \text{if } |m-n|\geq R_d\\ 0 & \text{if } |m-n|<R_d\end{cases}.
\end{aligned} \quad (52)$$

whith the same coefficients $a_p$ from (28).

## ACKNOWLEDGMENT

The authors thank the reviewers for their useful comments and suggestions and Dr. N. Pinel for his comments.

## REFERENCES

[1] C. Amra, G. Albrand, and P. Roche, "Theory and application of antiscattering single layers: Antiscattering antireflection coatings," *Appl. Opt.*, vol. 16, pp. 2695–2702, 1986.

[2] C. Amra, "Light scattering from multilayer optics. I. Tools of investigation," *J. Opt. Soc. Am. A*, vol. 11, pp. 197–210, 1994.

[3] C. Amra, "Light scattering from multilayer optics. II. Application to experiment," *J. Opt. Soc. Am. A*, vol. 11, pp. 211–226, 1994.

[4] I. Ohlidal and K. Navratil, "Scattering of light from multilayer systems with rough boundaries," *Phys. Opt.*, vol. 34, pp. 251–334, 1995.

[5] H. Kaplan, "Black coatings are critical in optical design," *Photon. Spectra*, vol. 31, pp. 48–50, 1997.

[6] R. Garcia-Llamas, L. E. Regalado, and C. Amra, "Scattering of light from a two-layer system with a rough surface," *J. Opt. Soc. Am. A*, vol. 16, no. 11, pp. 2713–2719, 1999.

[7] A. Soubret, "Diffusion des ondes electromagnétiques par des milieux et des interfaces aléatoires: étude des effets cohérents dans le champ diffusé," Ph.D. dissertation, Université de la Méditérranée, Aix-Marseille II, Centre de Physique théorique, France, 2001.

[8] A. Madrazo and A. A. Maradudin, "Numerical solutions of the reduced Rayleigh equation for the scattering of electromagnetic waves from rough dielectric films on perfectly conducting substrates," *Opt. Commun.*, vol. 134, pp. 251–263, 1997.

[9] V. Wismann, M. Gade, W. Alpers, and H. Hhnerfuss, "Radar signatures of marine mineral oil spills measured by an airborne multiradar," *Int. J. Remote Sens.*, vol. 19, pp. 3607–3623, 1998.

[10] H. A. Espedal and O. M. Johannessen, "Detection of oil spills near offshore installations using synthetic aperture radar (SAR)," *Int. J. Remote Sens.*, vol. 21, pp. 2141–2144, 2000.

[11] Z. Otremba and J. Piskozub, "Modelling of the optical contrast of an oil film on a sea surface," *Œ*, vol. 9, no. 12, pp. 411–416, 2001.

[12] D. Goodman and Conyers, *Ground Penetrating Radar, An Introduction for Archaeologists*. Walnut Creek, CA: Altamira, 1997.

[13] A. Tabatabaeenejad and M. Moghaddam, "Bistatic scattering from three-dimensional layered rough surfaces," *IEEE Trans. Geosci. Remote Sens.*, vol. 44, no. 8, pp. 2102–2114, 2006.

[14] A. Soubret, G. Berginc, and C. Bourrely, "Backscattering enhancement of an electromagnetic wave scattered by two-dimensional rough layers," *J. Opt. Soc. Am. A*, vol. 18, pp. 2778–2788, 2001.

[15] N. Pinel, N. Déchamps, C. Bourlier, and J. Saillard, "Bistatic scattering from one-dimensional random rough homogeneous layers in the high-frequency limit with shadowing effect," *Waves in Random Complex Media*, to be published.

[16] N. Déchamps, N. De Beaucoudrey, C. Bourlier, and S. Toutain, "Fast numerical method for electromagnetic scattering by rough layered interfaces: Propagation-inside-layer expansion method," *J. Opt. Soc. Am. A*, vol. 23, no. 2, pp. 359–369, 2006.

[17] C.-H. Kuo and M. Moghaddam, "Scattering from multilayer rough surfaces based on the extended boundary condition method and truncated singular value decomposition," *IEEE Trans. Antennas Propag.*, vol. 54, no. 10, pp. 2917–2929, 2006.

[18] C. D. Moss, T. M. Grzegorczyk, H. C. Han, and J. A. Kong, "Forward-backward method with spectral acceleration for scattering from layered rough surfaces," *IEEE Trans. Antennas Propag.*, vol. 54, no. 10, pp. 2917–2929, 2006.

[19] M. El-Shenawee, "Polarimetric scattering from two-layered two-dimensional random rough surfaces with and without buried objects," *IEEE Trans. Geosci. Remote Sens.*, vol. 42, no. 1, pp. 67–76, 2004.

[20] F. Harrington, *Field Computation by Moment Methods*. Piscataway, NJ: IEEE Press, 1993.

[21] L. Tsang, J. A. Kong, K.-H. Ding, and C. O. Ao, *Scattering of Electromagnetics Waves: Numerical Simulations*, ser. Wiley Series on Remote Sensing. New York: Wiley, 2001.

[22] M. Saillard and A. Sentenac, "Rigorous solution for electromagnetic scattering from rough surfaces," *Waves in Random Media*, vol. 11, pp. R103–R137, 2001.

[23] K. F. Warnick and W. C. Chew, "Numerical simulation methods for rough surface scattering: Topical review," *Waves in Random Media*, vol. 11, pp. R1–R30, 2001.

[24] E. I. Thorsos, "The validity of the Kirchhoff approximation for rough surface scattering using a Gaussian roughness spectrum," *J. Acoust. Soc. Am.*, vol. 83, no. 1, pp. 78–92, 1988.

[25] J. Q. Lu, A. A. Maradudin, and T. Michel, "Enhanced backscattering from a rough dielectric film on a reflecting substrate," *J. Opt. Soc. Am. B*, vol. 8, no. 2, pp. 311–318, 1991.

[26] W. H. Press, S. A. Teukolsky, W. T. Vetterling, and B. P. Flannery, *Numerical Recipies*, 2nd ed. Cambridge, U.K.: Cambridge Univ. Press, 1992.

[27] L. Tsang, C. H. Chan, K. Pak, and H. Sangani, "Monte-Carlo simulations of large-scale problems of random rough surface scattering and applications to grazing incidence with the BMIA/canonical grid method," *IEEE Trans. Antennas Propag.*, vol. 43, pp. 851–859, 1995.

[28] J. T. Johnson, "On the canonical grid method for two-dimensional scattering problems," *IEEE Trans. Antennas Propag.*, vol. 46, no. 3, pp. 297–302, 1998.
[29] C. H. Chan, L. Tsang, and Q. Li, "Monte-Carlo simulations of large-scale one-dimensional random rough-surface scattering at near-grazing incidence: Penetrable case," *IEEE Trans. Antennas Propag.*, vol. 46, no. 1, pp. 142–149, 1998.
[30] Q. Li, C. H. Chan, and L. Tsang, "Monte-Carlo simulations of wave scattering from lossy dielectric random rough surfaces using the physics-based two-grid method and the canonical-grid method," *IEEE Trans. Antennas Propag.*, vol. 47, no. 4, pp. 752–763, 1999.
[31] D. J. Donohue, H.-C. Ku, and D. R. Thompson, "Application of iterative moment-method solutions to ocean surfaces radar scattering," *IEEE Trans. Antennas Propag.*, vol. 46, no. 1, pp. 121–132, 1998.
[32] V. Rokhlin, "Rapid solution of integral equations of scattering theory in two dimensions," *J. Comput. Phys.*, vol. 36, pp. 414–439, 1990.
[33] D. A. Kapp and G. S. Brown, "A new numerical method for rough-surface scattering calculations," *IEEE Trans. Antennas Propag.*, vol. 44, no. 5, pp. 711–722, 1996.
[34] R. J. Adams and G. S. Brown, "An iterative solution of one-dimensional rough surface scattering problems based on a factorization of the Helmholtz operator," *IEEE Trans. Antennas Propag.*, vol. 47, no. 4, pp. 765–767, 1999.
[35] D. Holliday, L. L. DeRaad, Jr., and G. J. St-Cyr, "Forward-backward method for scattering from imperfect conductors," *IEEE Trans. Antennas Propag.*, vol. 46, no. 1, pp. 101–107, 1998.
[36] H.-T. Chou and J. T. Johnson, "A novel acceleration algorithm for the computation of scattering from rough surfaces with the forward-backward method," *Radio Sci.*, vol. 33, pp. 1277–1287, 1998.
[37] H.-T. Chou and J. T. Johnson, "Formulation of forward-backward method using novel spectral acceleration for the modeling of scattering from impedance rough surfaces," *IEEE Trans. Geocis. Remote Sens.*, vol. 38, no. 1, pp. 605–607, 2000.
[38] D. Torrungrueng and J. T. Johnson, "Some issues related to the novel spectral acceleration method for the fast computation of radiation/scattering from one-dimensional extremely large scale quasi-planar structures," *Radio Sci.*, vol. 37, no. 2, 2002.
[39] M. Abramowitz and I. A. Stegun, *Handbook of Mathematical Functions*. Washington, DC: U. S. Dept. Commerce, 1970.
[40] I. Gohberg and V. Olshevsky, "Complexity of multiplication with vectors for structured matrices," *Linear Algebra. Appl.*, vol. 202, pp. 163–192, 1994.

**Nicolas Déchamps** was born in Provins, France, in 1977. He received the Engineering Degree from Ecole Centrale de Nantes, Nantes, France, the M.Sc. degree in automation and applied computer science from the Communications and Cybernetic Research Institute of Nantes (IRCCyN), and the Ph.D. degree in physics from the Institut de Recherche en Electrotechnique et Electronique de Nantes Atlantique, (IREENA), Polytech'Nantes, in 2001 and 2004, respectively.

After a postdoctoral position at the Pulp and Paper Center at the University of Toronto, Canada, where he worked on optical properties of paper, he joined the radar team of IREENA Laboratory as a Research Associate in 2006. His research interest includes fast methods for numerical simulations of scattering from multilayers separated by rough interfaces and analytical modelling of paper gloss.

**Christophe Bourlier** (M'99) was born in La Fléche, France, on July 6, 1971. He received the M.S. degree in Electronics from the University of Rennes (France), in 1995 and the Ph.D. degree from the Système Electronique et Informatique, Nantes, France, in 1999

While at the University of Rennes, he was with the Laboratory of Radiocommunication where he worked on antenna coupling in the VHF-HF band. Currently, he is with the Institut de Recherche en Electrotechnique et Electronique de Nantes Atlantique (IREENA) Laboratory, on the Radar Team at Polytech'Nantes (University of Nantes, France). He works as an Assistant Researcher at the National Center for Scientific Research on electromagnetic wave scattering from rough surfaces and objects for remote sensing applications. He is the author of more than 80 journal articles and conference papers.